IEEE Photonics Journal
An IEEE Photonics Society Publication

Ge-Doped Microstructured Multicore Fiber for Customizable Supercontinuum Generation

Volume 3, Number 6, December 2011

Daniele Modotto, Member, IEEE
Gabriele Manili
Umberto Minoni, Member, IEEE
Stefan Wabnitz, Member, IEEE
Costantino De Angelis, Member, IEEE
Graham Town, Senior Member, IEEE
Alessandro Tonello
Vincent Couderc

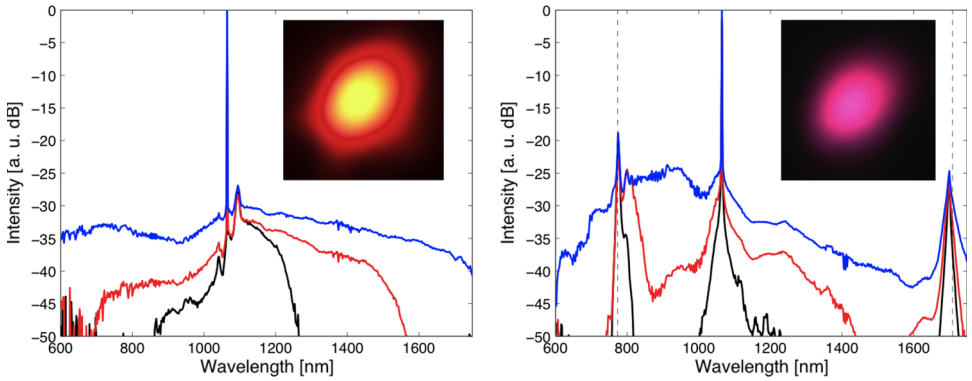

DOI: 10.1109/JPHOT.2011.2175211
1943-0655/$26.00 ©2011 IEEE

Ge-Doped Microstructured Multicore Fiber for Customizable Supercontinuum Generation

Daniele Modotto,[1] *Member, IEEE*, Gabriele Manili,[1] Umberto Minoni,[1] *Member, IEEE*, Stefan Wabnitz,[1] *Member, IEEE*, Costantino De Angelis,[1] *Member, IEEE*, Graham Town,[2] *Senior Member, IEEE*, Alessandro Tonello,[3] and Vincent Couderc[3]

[1]Dipartimento di Ingegneria dell'Informazione, Università degli Studi di Brescia, 25123 Brescia, Italy
[2]Department of Electronic Engineering, Macquarie University, Sydney, NSW 2109, Australia
[3]XLIM, Université de Limoges, UMR CNRS 6172, 87060 Limoges, France

DOI: 10.1109/JPHOT.2011.2175211

Manuscript received September 30, 2011; revised November 2, 2011; accepted November 2, 2011. Date of publication November 8, 2011; date of current version December 2, 2011. Corresponding author: D. Modotto (e-mail: daniele.modotto@ing.unibs.it).

Abstract: Supercontinuum generation in a multicore fiber in which several uncoupled cores were doped with dissimilar concentrations of germanium was studied experimentally. Germanium doping provided control over the separation between the zero-dispersion wavelength and the 1064-nm wavelength of a Q-switched Nd:YAG pump laser. Supercontinua generated independently in each core of the same piece of fiber displayed clear and repeatable differences due to the influence of germanium doping on refractive index and four-wave mixing. The spectral evolution of the subnanosecond pump pulses injected into the different cores was accurately reproduced by numerical simulations.

Index Terms: Supercontinum generation, fiber nonlinear optics, four-wave mixing.

1. Introduction

Microstructured optical fibers (MOFs) are ideal components to observe cubic nonlinear optical phenomena [1]. In fact, the possibility of controlling the position of the zero-dispersion wavelength (ZDW) by changing the geometrical parameters of the fiber cross section and the small core effective area are key factors to enhance the effective nonlinearity and to choose which nonlinear phenomena will play a predominant role. Self-phase modulation (SPM), modulation instability (MI), cross-phase modulation (XPM), four-wave mixing (FWM), and stimulated Raman scattering (SRS) are the major factors when the nonlinear evolution of nanosecond or picosecond pulses along a MOF are considered [1], [2]. These phenomena are often present at the same time and can lead to the extremely wide spectral broadening or supercontinuum (SC) at the fiber output. SC generation has been studied in several fibers and for different pumping conditions; experiments show that the spectral density at the output of the fiber can reach remarkable values from the visible to the infrared part of the electromagnetic spectrum [3], [4].

The features of the SC spectra, and in particular the presence of the FWM peaks and their spectral separation from the pump, can be tuned by engineering the MOF fiber cross section design [5] or by utilizing germanium or lanthanum doped silica based glasses [6]–[8]. In our work, we use an MOF whose cores were doped with germanium. An increase in the refractive index of the core as large as 0.08 has been reported for a doping of 55 mol.% GeO_2 [9], and values of 0.03–0.05 are readily

technologically accessible [7], [9]. Light is guided by the refractive index difference between glass and air and not by the presence of a photonic band gap, as in the case of photonic crystal fibers [10]–[12]. Moreover, the nonlinear coefficient is almost linearly dependent on the concentration of germanium and a value of $n_2 = 3.0 \times 10^{-16}$ cm^2/W is reached for a concentration of 30 mol.% GeO_2 [13], [14], which represents an increase of almost 40% with respect to the value of $n_2 = 2.16 \times 10^{-16}$ cm^2/W reported for plain silica glass [13]. Ge-doped fibers are well suited to the FWM process when the pump laser is few tens of nanometer away from the ZDW and in the normal dispersion region. For example, efficient FWM process leading to the formation of a Stokes band at 2250 nm and an anti-Stokes band at 704 was described in [15], and wavelength conversion from 813 nm to 1540 nm with a pump at 1064 nm was reported in [16].

Because the output spectral features can be controlled by the germanium concentration, MOFs having the same geometrical structure can generate different supercontinua starting from the same pump laser. In this paper, we developed this idea further and designed a multicore fiber whose cores exhibit almost the same cross section but have different levels of germanium doping. The microstructured multicore optical fiber (MMOF) under study is an ideal test-bench to assess the influence of doping on SC generation, but it is also a first step toward the engineering of a compact device capable of emitting different SC spectra. Due to the short distance among the cores, the input beam can easily be switched from one core to another [17].

Multicore fibers have already been proposed and tested as curvature or bend sensors [18], [19] and as transmission media for spatial mode multiplexed optical networks [20], [21]. They have also been used to manufacture phase-locked high power lasers [22]. Our multicore SC source can benefit from these previous scientific and technological achievements. For example, tapered multicore fiber connectors [20] can be used to easily access the input and output of each core of the MMOF, and substantial advances in the inscription of dielectric waveguides by high-power fs-lasers enables the fabrication of waveguide arrays [23] for coupling with each individual core of the MMOF or to combine the MMOF outputs into a single waveguide.

2. Ge-Doped Microstructured Fiber and Experimental Setup

We designed a seven-core MMOF whose cores are not linearly coupled for wavelengths between visible and near-infrared ($\lambda < 1.75$ μm); in such a way, the MMOF is basically a bunch of seven closely packed fibers. The fiber was fabricated at PERFOS laboratories starting from glass capillary tubes and rods by using a stack-and-draw method [10], [24]–[26]. A scanning electron microscope (SEM) image of the fiber cross section is displayed in Fig. 1(a). The hexagonal pattern of holes is slightly perturbed by two large central holes and by the fact that the holes toward the center of the fiber have slightly smaller radii. Three of the cores are closer to the central holes and are strongly birefringent; in such cores, it is possible to observe intermodal and vectorial FWM, as it has previously been reported for similar MOFs [4], [17].

In this paper, we focus our attention on the four most external cores, in particular on the cores numbered 1, 2, and 3 and highlighted by white circles in Fig. 1(a); the fourth outer core has the same characteristics of core 1, and thus, its analysis will not be reported. Close inspection of the SEM image reveals that these cores have almost the same geometrical shape, but they differ in their level of germanium doping; while core 1 is undoped, the germanium in cores 2 and 3 leads to an increase in the host glass refractive indices of $\Delta n = 0.0125$ and $\Delta n = 0.025$, respectively. The radius of the doped region in each core is assumed equal to 1125 nm. These values of Δn and doping radius have been obtained starting from the measured positions of the FWM peaks (which are described in the following section) and are in close agreement with the values expected from our knowledge of the doping process and stack-and-draw technique. By extracting the lattice geometry from the SEM image and utilizing a finite-element method (FEM) mode solver [27], we calculated the modes at the pump wavelength and verified that the three cores support two LP_{01} modes (one for each polarization); in our study, the LP_{11} modes are not relevant. As can be intuitively predicted from the SEM image, and as confirmed by our mode solver, the cores are birefringent with their principal axes oriented at approximately 45° and 135° with respect to the x axis

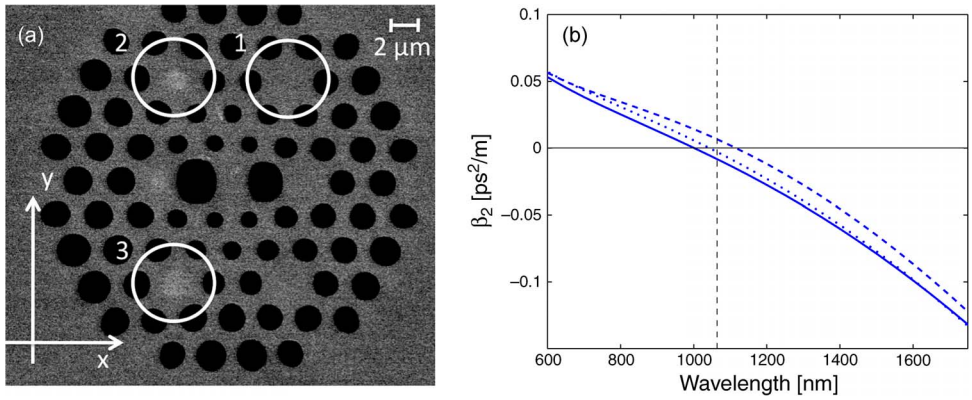

Fig. 1. (a) Scanning electron microscope (SEM) image of the MMOF; the cores under study are circled in white. (b) Dispersion curves (β_2) for $LP_{01,45^\circ}$ in core 1 (solid line), $LP_{01,135^\circ}$ in core 2 (dotted line), and $LP_{01,135^\circ}$ in core 3 (dashed line). The vertical dashed line corresponds to the pump wavelength (1064 nm).

[see the reference system in Fig. 1(a)]. Using the mode solver, we calculated the effective indices and the dispersion curves of the LP_{01} modes of the three cores. Fig. 1(b) shows the dispersion curves for $LP_{01,45^\circ}$ in core 1 (undoped core), for $LP_{01,135^\circ}$ in core 2 (doped core), and $LP_{01,135^\circ}$ in core 3 (most doped core); the predicted ZDWs are 1001 nm, 1043 nm, and 1115 nm, respectively. Increasing the germanium concentration shifted the ZDW toward longer wavelengths, and we have demonstrated that shifts in excess of 100 nm are feasible by this method. It has been reported in a recent work that the concentration of germanium also changes the dispersion slope [28].

We experimentally studied SC generation in the three cores by using as pump source a microchip Nd:YAG Q-switched laser working at 1064 nm [2] and emitting pulses with a duration of 600 ps and an estimated maximum peak power of 6 kW. The laser output was coupled into a single core by a microlens $(f = 4.5\ \text{mm}, \text{NA} = 0.42)$; a micrometric 3-axis stage permitted us to carefully focus the beam on the input facet of the selected core and to easily move the excitation from one core to an adjacent one without changing the coupling efficiency. A neutral density filter, a linear polarizer and a half-wave plate were inserted along the optical path between the laser and the focusing stage to precisely control both the power level and the linear polarization of the input beam. At the fiber output end, the optical power was monitored by means of a broadband power sensor, and a digital camera was used to inspect the far-field shape of the visible part of the SC spectra carried by each core. Using a bare fiber adapter the output facet of the MMOF could be connected to a spectrum analyzer (Anritsu MS9710C) with range 600–1750 nm.

3. Results and Discussion

In this section the spectra at the output of the different cores of our 3-m-long fiber are presented. It is also shown how the spectral features change with the level of the core doping. The output spectra were recorded at different values of the input power; the spectral resolution was set to 0.1 nm for all of the measured spectra that are reported below. The peak power of the pulses that were injected in the core under study has been estimated by measuring the laser output average power and from the knowledge of both the pulse duration and the laser repetition rate.

Let us start by analyzing the undoped core 1. The measured spectra for the peak powers of 200 W, 400 W, and 1400 W are depicted in Fig. 2(a); to facilitate the comparison among different levels of power, these spectra are normalized to the maximum of the most intense spectrum. Since the pump lies in the anomalous dispersion region [see the solid line in Fig. 1(b)], when the input power grows larger, the pump spectral line starts to develop MI peaks and to broaden; the MI peaks are clearly recognizable at the wavelength of 1082 nm and 1050 nm. By further increasing the pump power up to 400 W, the output spectrum exhibits a long tail: this is due to the fact that MI breaks the long input pulse, giving rise to very intense and high-order solitons which are red-shifted due to

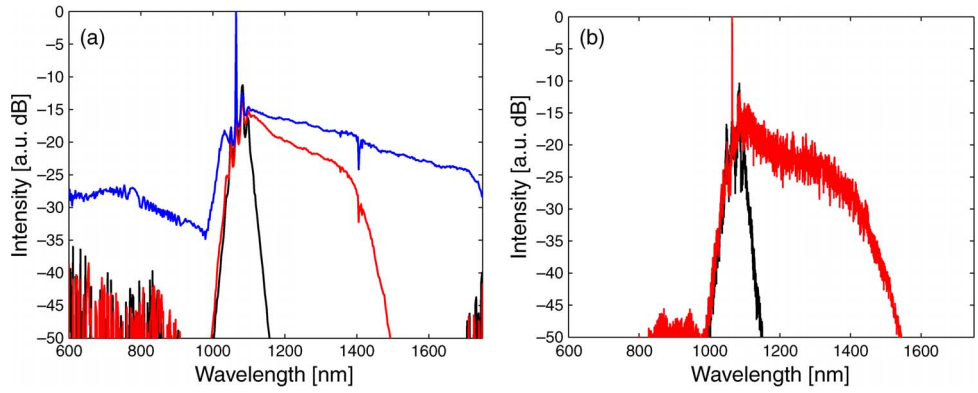

Fig. 2. (a) Measured spectra at the output of core 1 for three peak powers: 200 W (black), 400 W (red), and 1400 W (blue); the input is polarized at 45° with respect to the x axis. (b) BPM results for the peak powers 200 W and 400 W.

SRS. For an input power of 1400 W, the output spectrum extends to 1700 nm, and some power is also present in the visible part of the spectrum.

To verify our understanding of the processes leading to the formation of the SC spectrum, we simulated the evolution of the pulses inside each core by solving the Generalized Nonlinear Schrödinger Equation [1] by means of a split-step based Beam Propagation Method (BPM). Our code includes both the instantaneous (Kerr) and delayed (Raman) contributions to the fiber cubic nonlinearity as well as the full dispersion curve, as calculated by the mode solver. Self-steepening and linear fiber losses were not included in our code.

It should be emphasized that the simulation of 600-ps-long pulses giving rise to more than 1000-nm-wide bandwidth involves an enormous computational cost. In the numerical results reported here we used a 4320 ps wide temporal domain window that was sampled at 2^{21} points, and the propagation step along z was equal to 50 μm. The initial noise was estimated by using the one-photon per mode model [1]. As the calculated spectra were quite noisy, they were cleaned by filtering the output via a moving average filter, simulating the limited resolution of the optical spectrum analyzer (OSA). The spectra measured by the OSA show the spectral densities averaged over many pulses and thus, in principle, to compare the numerical results to the experiments, we should also calculate the average of several spectra obtained from different random realizations of the input noise. Due to the computational burden required for a single simulation, this approach was not viable; hence, the spectra resulting from the simulations are evidently more noisy compared with the measured ones.

The spectra calculated for the peak powers 200 W and 400 W are plotted in Fig. 2(b), in which both the MI peaks and the long infrared tail are in excellent agreement with the experiment. The nonlinear coefficient used for the simulations was $\gamma = 22\ \mathrm{W}^{-1} \cdot \mathrm{km}^{-1}$. Simulations corresponding to the highest level of power (1400 W) were not performed because in presence of such wide spectral broadening, we believe that our numerical results are no longer fully reliable; in fact, to include the visible frequencies, mid infrared (MIR) frequencies beyond 2 μm must be included as well; however, data for the fiber dispersion were not available in the MIR frequency range. Most importantly, losses cannot be neglected for wavelengths larger than 1700 nm so that frequency dependent losses should be added to our numerical code.

The spectra observed in the low-doped core 2 $(\Delta n = 0.0125)$ are remarkably different from the undoped case even if the pump is still located in the anomalous dispersion region. As can be observed in Fig. 3(a) for power levels lower than 1000 W, the spectra (whose broadening is initiated by MI) develop a tail toward the infrared, but at the same time, noticeable power is also transferred toward the visible. Extensive numerical simulations, partially reported in Fig. 3(b), show that signal appears in the visible once the spectral region to the right of the pump is filled; the latter is a result of the pump wavelength being very close to the ZDW (1043 nm). At the maximum level of power which

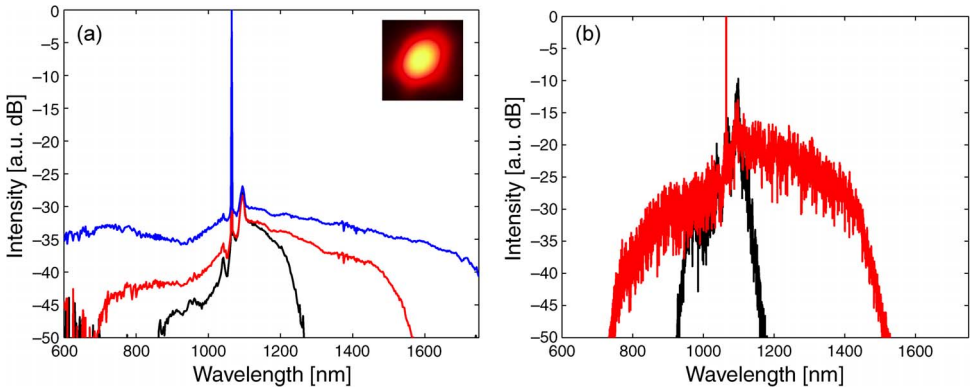

Fig. 3. (a) Measured spectra at the output of core 2 for 3 peak powers: 300 W (black), 600 W (red), and 1900 W (blue); the input is polarized at 135° with respect to the x axis. (b) BPM results for the peak powers 300 W (black) and 600 W (red).

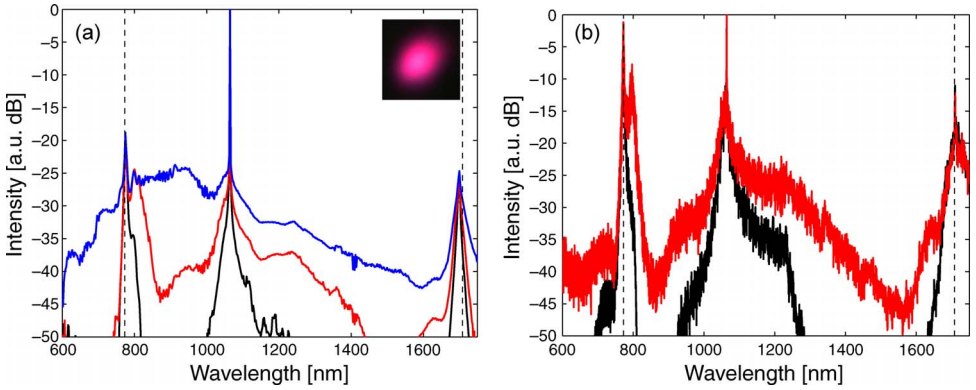

Fig. 4. (a) Measured spectra at the output of core 3 for three peak powers: 600 W (black), 1100 W (red), and 2800 W (blue); the input is polarized at 135° with respect to the x axis. (b) BPM results for the peak powers 600 W (black) and 1100 W (red).

is reported in Fig. 3(a), the visible spectral density is only 5 dB lower than the infrared immediately to the right of the pump. At levels of power larger than 200 W, the MMOF turns red-orange; the inset of Fig. 3(a) shows a photograph of the far field of the mode as it appears when it is projected on a screen. The almost circular shape proves that the visible light is carried by the $LP_{01,135^\circ}$ mode (with the electric field polarized at 135° with respect to x).

On the other hand, the spectra observed at the output of the highly-doped core 3 ($\Delta n = 0.025$) are expected to be different from the previous cases as the pump now lies in the normal region, leading to the presence of FWM peaks. Indeed, Fig. 4(a) shows the output spectra for three powers (600 W, 1100 W, and 2800 W) in which the FWM peaks are clearly recognizable. For the mode which is polarized at 135°, the Stokes line is at 1692 nm, and the anti-Stokes line lies at 776 nm. Using the numerically calculated effective refractive indices and the FWM phase-matching relation [2], the peak positions are predicted at 1708 nm and 773 nm. The close agreement between the experimental and expected location of the FWM peaks confirms the correctness of the chosen values to model the Ge-doped rod (Δn and rod radius). When the input beam was polarized at 45°, we observed at the output the anti-Stokes peak at 758 nm only, since the corresponding Stokes wavelength is 1784 nm, which is beyond the measuring range of our OSA. We observed that at peak powers higher than 1000 W, the spectral density rises both in the region between the pump and the Stokes line and in the region between the pump and the anti-Stokes peak, and this is true for both polarizations. The image of the visible light carried by core 3 at the maximum level of power (2800 W)

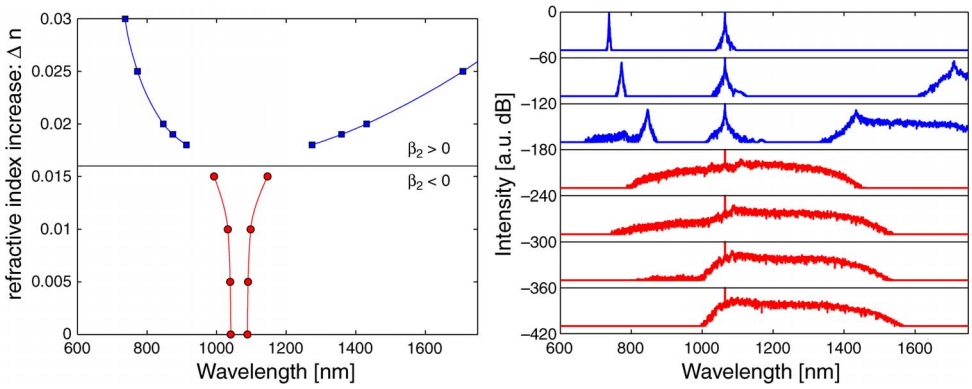

Fig. 5. (Left) Calculated positions of spectral peaks as a function of the refractive index increase Δn (due to the doping); red refers to MI peaks in the anomalous dispersion regime, and blue refers to FWM peaks in the normal dispersion regime. (Right) BPM calculated spectra for an input peak power of 500 W when the core refractive index is increased by (from bottom to top) $\Delta n = 0, 0.005, 0.01, 0.015, 0.02,$ 0.025, and 0.03.

as it was projected on a screen is displayed in the inset of Fig. 4(a). The pump and both Stokes and anti-Stokes peaks are transported by the almost round $LP_{01,135^\circ}$ mode. Cores designed with a proper level of doping could be used for light sources based on FWM since the emitted wavelength can be tuned during the fiber design by suitably choosing the level of doping.

To verify how finely the output spectra can be tuned by means of increasing the refractive index difference between the core and the surrounding glass, as a first step, we calculated the dispersion curves (via the FEM tool) for refractive index differences Δn between 0 and 0.03, i.e., the range that is technologically accessible. The pump wavelength was reasonably fixed at the wavelength of 1064 nm, so that, by increasing Δn, the sign of β_2 at the pump wavelength changes from negative to positive at around $\Delta n = 0.016$. The spectral broadening is initiated by MI whenever the pump lies in the anomalous regime whereas if the pump is in the normal regime, power is transferred from the narrow band input pulses to the FWM peaks. The left part of Fig. 5 shows the predicted positions of the MI peaks (red) and of the FWM peaks (blue) for different values of Δn; the nonlinear term in the FWM phase-matching relation was neglected since, for all peak power levels of the Nd:YAG microchip laser, its contribution remains very small when compared to the linear term. As a test, we simulated the evolution of pulses with a time duration of 600 ps and a peak power of 500 W along a 3 m long fiber whose geometry is that of core 3, but whose refractive index is increased by $\Delta n = 0, 0.005, 0.01, 0.015, 0.02, 0.025,$ and 0.03; the results are reported in the right part of Fig. 5. The red spectra are those obtained for a pump in the anomalous region $(\Delta n \leq 0.015)$; the spectral evolution in the initial section of the fiber (not shown here) clearly shows the MI peaks, whose signature remains still appreciable in the output spectra. The blue lines refer to a pump in the normal regime $(\Delta n \geq 0.02)$; here, the onset of FWM peaks gives rise to a wider final spectrum at the expense of a less-uniform spectral density since, at the chosen level of input power, the spectral broadening is not sufficient to entirely fill up the spectral regions between the pump and the FWM peaks.

4. Conclusion

MMOFs can be engineered to generate different SC spectra from the same pump laser. In particular, by carefully choosing the distance between the pump wavelength and the ZDW, the presence and the positions of Stokes and anti-Stokes bands can be controlled. The ZDW can be selected during the design by adding germanium in the glass. Our experiments with three cores of a seven-core fiber confirm the validity of this approach. The observed spectral peak positions are in agreement with the predictions based on the FWM phase-matching relation for each polarization.

Extensive numerical simulations reproduce all the spectra details, and their evolution as the input power is increased.

Recent technological advances suggest that such multicore fibers could provide the enabling technology for developing tunable laser sources capable of producing different SC spectra or different intense near infrared (or visible) peaks in the *L–C* bands. Obviously, such tuning action is obtained by selectively exciting only one core and by collecting the spectrum at the output facet of the selected core. In principle, by connecting the output cores to an integrated circuit working as a beam combiner, the spectra generated in more than one core could be combined in a single output waveguide, thus opening the possibility of obtaining a SC spectrum which represents a linear superposition of the different SC spectra from each individual core.

References

[1] J. M. Dudley, G. Genty, and S. Coen, "Supercontinuum generation in photonic crystal fiber," *Rev. Mod. Phys.*, vol. 78, no. 4, pp. 1135–1184, Oct.–Dec. 2006.

[2] W. J. Wadsworth, N. Joly, J. C. Knight, T. A. Birks, F. Biancalana, and P. St. J. Russell, "Supercontinuum and four-wave mixing with Q-switched pulses in endlessly single-mode photonic crystal fibres," *Opt. Exp.*, vol. 12, no. 2, pp. 299–309, Jan. 2004.

[3] J. M. Stone and J. C. Knight, "Visibly 'white' light generation in uniform photonic crystal fiber using a microchip laser," *Opt. Exp.*, vol. 16, no. 4, pp. 2670–2675, Feb. 2008.

[4] C. Lesvigne, V. Couderc, A. Tonello, P. Leproux, A. Barthélémy, S. Lacroix, F. Druon, P. Blandin, M. Hanna, and P. Georges, "Visible supercontinuum generation controlled by intermodal four-wave mixing in microstructured fiber," *Opt. Lett.*, vol. 32, no. 15, pp. 2173–2175, Aug. 2007.

[5] A. Labruyère, A. Martin, P. Leproux, V. Couderc, A. Tonello, and N. Traynor, "Controlling intermodal four-wave mixing from the design of microstructured optical fibers," *Opt. Exp.*, vol. 16, no. 26, pp. 21 997–22 002, Dec. 2008.

[6] Y. P. Yatsenko and A. D. Pryamikov, "Parametric frequency conversion in photonic crystal fibres with germanosilicate core," *J. Opt. A, Pure Appl. Opt.*, vol. 9, no. 7, pp. 716–722, Jul. 2007.

[7] V. Tombelaine, A. Labruyère, J. Kobelke, K. Schuster, V. Reichel, P. Leproux, V. Couderc, R. Jamier, and H. Bartelt, "Nonlinear photonic crystal fiber with a structured multi-component glass core for four-wave mixing and supercontinuum generation," *Opt. Exp.*, vol. 17, no. 18, pp. 15 392–15 401, Aug. 2009.

[8] J. Kobelke, K. Schuster, D. Litzkendorf, A. Schwuchow, J. Kirchhof, V. Tombelaine, H. Bartelt, P. Leproux, V. Couderc, A. Labruyère, and R. Jamier, "Highly germanium and lanthanum modified silica based glasses in microstructured optical fibers for non-linear applications," *Opt. Mater.*, vol. 32, no. 9, pp. 1002–1006, Jul. 2010.

[9] Y. P. Yatsenko, A. D. Pryamikov, V. M. Mashinsky, M. E. Likhachev, A. O. Mavritsky, E. M. Dianov, A. N. Guryanov, V. F. Khopin, and M. Y. Salgansky, "Four-wave mixing with large Stokes shifts in heavily Ge-doped silica fibers," *Opt. Lett.*, vol. 30, no. 15, pp. 1932–1934, Aug. 2005.

[10] P. S. J. Russell, "Photonic crystal fibers," *Science*, vol. 299, no. 5605, pp. 358–362, Jan. 2003.

[11] P. S. J. Russell, "Photonic-crystal fibers," *J. Lightw. Technol.*, vol. 24, no. 12, pp. 4729–4749, Dec. 2006.

[12] J. C. Knight, "Photonic crystal fibers and fiber lasers (invited)," *J. Opt. Soc. Amer. B*, vol. 24, no. 8, pp. 1661–1668, Aug. 2007.

[13] Y. P. Yatsenko and A. Mavritsky, "D-scan measurement of nonlinear refractive index in fibers heavily doped with GeO_2," *Opt. Lett.*, vol. 32, no. 22, pp. 3257–3259, Nov. 2007.

[14] K. Nakajima and M. Ohashi, "Dopant dependence of effective nonlinear refractive index in GeO_2- and F-doped core single-mode fibers," *IEEE Photon. Technol. Lett.*, vol. 14, no. 4, pp. 492–494, Apr. 2002.

[15] A. Labruyère, P. Leproux, V. Couderc, V. Tombelaine, J. Kobelke, K. Schuster, H. Bartelt, S. Hilaire, G. Huss, and G. Mélin, "Structured-core GeO_2-doped photonic-crystal fibers for parametric and supercontinuum generation," *IEEE Photon. Technol. Lett.*, vol. 22, no. 16, pp. 1259–1261, Aug. 2010.

[16] Y. P. Yatsenko, A. F. Kosolapov, A. E. Levchenko, S. L. Semjonov, and E. M. Dianov, "Broadband wavelength conversion in a germanosilicate-core photonic crystal fiber," *Opt. Lett.*, vol. 34, no. 17, pp. 2581–2583, Sep. 2009.

[17] G. Manili, D. Modotto, U. Minoni, S. Wabnitz, C. De Angelis, G. Town, A. Tonello, and V. Couderc, "Modal four-wave mixing supported generation of supercontinuum light from the infrared to the visible region in a birefringent multi-core microstructured optical fiber," *Opt. Fiber Technol.*, vol. 17, no. 3, pp. 160–167, May 2011.

[18] W. N. MacPherson, M. J. Gander, R. McBride, J. D. C. Jones, P. M. Blanchard, J. G. Burnett, A. H. Greenaway, B. Mangan, T. A. Birks, J. C. Knight, and P. St. J. Russell, "Remotely addressed optical fibre curvature sensor using multicore photonic crystal fibre," *Opt. Commun.*, vol. 193, no. 1–6, pp. 97–104, Jun. 2001.

[19] G. M. H. Flockhart, W. N. MacPherson, J. S. Barton, J. D. C. Jones, L. Zhang, and I. Bennion, "Two-axis bend measurement with Bragg gratings in multicore optical fiber," *Opt. Lett.*, vol. 28, no. 6, pp. 387–389, Mar. 2003.

[20] B. Zhu, T. F. Taunay, M. F. Yan, J. M. Fini, M. Fishteyn, E. M. Monberg, and F. V. Dimarcello, "Seven-core multicore fiber transmissions for passive optical network," *Opt. Exp.*, vol. 18, no. 11, pp. 11 117–11 122, May 2010.

[21] B. Zhu, T. F. Taunay, M. F. Yan, M. Fishteyn, G. Oulundsen, and D. Vaidya, "70-Gb/s multicore multimode fiber transmissions for optical data links," *IEEE Photon. Technol. Lett.*, vol. 22, no. 22, pp. 1647–1649, Nov. 2010.

[22] L. Li, A. Schülzgen, H. Li, V. L. Temyanko, J. V. Moloney, and N. Peyghambarian, "Phase-locked multicore all-fiber lasers: Modeling and experimental investigation," *J. Opt. Soc. Amer. B*, vol. 24, no. 8, pp. 1721–1728, Aug. 2007.

[23] R. R. Thomson, H. T. Bookey, N. D. Psaila, A. Fender, S. Campbell, W. N. MacPherson, J. S. Barton, D. T. Reid, and A. K. Kar, "Ultrafast-laser inscription of a three dimensional fan-out device for multicore fiber coupling applications," *Opt. Exp.*, vol. 15, no. 18, pp. 11 691–11 697, Sep. 2007.
[24] L. Brilland, F. Smektala, G. Renversez, T. Chartier, J. Troles, T. N. Nguyen, N. Traynor, and A. Monteville, "Fabrication of complex structures of holey fibers in chalcogenide glass," *Opt. Exp.*, vol. 14, no. 3, pp. 1280–1285, Feb. 2006.
[25] T. Y. Cho, G. H. Kim, K. Lee, and S. B. Lee, "Study on the fabrication process of polarization maintaining photonic crystal fibers and their optical properties," *J. Opt. Soc. Korea*, vol. 12, no. 1, pp. 19–24, Mar. 2008.
[26] N. J. Traynor, A. Monteville, L. Provino, D. Landais, O. Le Goffic, T. N. Nguyen, T. Chartier, D. Tregoat, and J. C. Travers, "Fabrication and applications of low loss nonlinear Holey fibers," *Fiber Integr. Opt.*, vol. 28, no. 1, pp. 51–59, Feb. 2009.
[27] COMSOL Multiphysics. [Online]. Available: http://www.comsol.com
[28] B. Barviau, O. Vanvincq, A. Mussot, Y. Quiquempois, G. Mélin, and A. Kudlinski, "Enhanced soliton self-frequency shift and CW supercontinuum generation in GeO_2-doped core photonic crystal fibers," *J. Opt. Soc. Amer. B*, vol. 28, no. 5, pp. 1152–1160, May 2011.